Radiation Quality Evaluation of Orbita HyperSpectral Image

Lifu Zhang (1), Sa Wang (1)(2), Linshan Zhang (1)(2)

[1]Aerospace Information Research Institute, Chinese Academy of Sciences, 20 Datun road, Chaoyang District, Beijing, 100049, China

[2] University of Chinese Academy of Sciences, 19 Yuquan Road, Shijingshan District, Beijing, 100049, China

Email: zhanglf@radi.ac.cn; wangsa@aircas.ac.cn; zhangls@aircas.ac.cn

KEY WORDS: Orbita Hyper Spectral, Radiation accuracy, Image definition, Signal to Noise Ratio, Shannon Entropy

ABSTRACT: The Orbita Hyper Spectral (OHS)-2 and 3 satellites were successfully launched on April 26, 2018 and September 19, 2019, respectively. The basis of remote sensing data applications is the data quality evaluation. Rradiation accuracy, image definition, signal to noise ratio (SNR) and entropy were selected as evaluating indicators, the radiation quality of OHS level 1 images were evaluated, and the radiation quality of OHS-2A and OHS-3D were compared. The results showed that the image definition (EVA) of each band of OHS-2A is above 24. The signal-to-noise ratio (SNR) is between 1-14 and the information entropy (H) is above 5.4. The SNR of the 466-686nm spectral showed a decreasing trend, especially in the 686nm spectrum, the SNR showed a minimum value. Each band definition of OHS-3D is above 16, and SNR is between 1-37, while the entropy is 4.5 above. In the 896nm-940nm (29-32 bands) spectrum, the entropy and definition showed a decreasing trend. At the same time, at 940nm (32 band), the minimum values of the entropy and definition appeared, while the OHS hyperspectral data has a high information entropy than EO-1 Hyperion hyperspectral data and HJ1B data, and they all showed the same level in SNR and information entropy. In blue (466-520nm), green (536-596nm), red (610-730nm) and infrared spectrum (746-940nm), the maximum and average values of SNR, definition and entropy of OHS-3D were all greater than that of OHS-2A. In general, the radiation of OHS-3D is better than that of OHS-2A. In the application of OHS-3D images, the last 4 bands (29-32 bands) could be abandoned. Due to the high spatial resolution (10m) and high temporal resolution (2 days) ,OHS plays an irreplaceable role in agricultural remote sensing and inland/coastal water quality monitoring.

1. INTRODUCTION

Zhuhai-1 is the first micro-nano satellite constellation launched by a private enterprise in China. It consists of 34 satellites, including video satellites and hyperspectral satellites. A total of 10 Orbita HyperSpectral (OHS) satellites are planned, with 4 OHS-2 satellites successfully launched on April 26, 2018, and 4 OHS-3 satellites successfully launched on September 19, 2019. OHS adopts push scan imaging method, with the spatial resolution of 10 m, spectral resolution of 2.5nm and wavelength range of 400-1000nm(32 bands), It could choose other bands for downlink through the command, whose width is 150 km by 150 km and orbit at 98º the sun synchronous with a altitude of 500 km. It supports the on-orbit calibration at the same time, ideally total 10 satellites once every 2 days can be global coverage (Hong 2019; Li et al., 2019). At present, OHS data have been successfully applied in soil organic matter content inversion, inland water body area extraction, water body parameter inversion, and crop fine classification, etc. (Hong 2019; Sun et al., 2020; Yin

2020; Zhang 2019).

Remote sensing data quality evaluation is the basis of remote sensing data application and has been paid much attention by many experts. Methods of remote sensing data quality evaluation are divided into subjective and objective evaluation methods (He et al., 2017; Wang et al., 2016; Yin et al., 2014; Zhou et al., 2008). Subjective evaluation, namely visual evaluation, mainly relies on visual inspection to rate the quality of the image. The subjective evaluation method mainly relies on the subjective feeling of the person. However, due to the different experience, quality, cognitive level and personal background of each person, different evaluators may have different evaluation results of the same image. Meanwhile, the subjective evaluation method is also limited by the discrimination ability of human eyes (Cao, 2014; Zeng 2017; Ren 2008). In order to ensure the correctness of the subjective evaluation results, at least 20 personnel should participate in the subjective evaluation (Ren 2008). At present, international standards have been set for the subjective evaluation methods of multimedia applications and television images: ITU-T REC.P.910 and ITU-R BT.500-11. However, there is no unified standard for the subjective evaluation of the quality of hyperspectral data. The objective evaluation method is based on the physical characteristics of the image and carries out quantitative evaluation with specific indicators, which can avoid the subjective problems existing in the subjective evaluation method.

Many scholars evaluated the quality of hyperspectral data based on objective evaluation methods: Forster and Best (1994) analyzed the quality of SPOT images through modulation transfer function; Kamal et al. (2016) compared the data quality of WorldView-2, ALOS Avnir-2 and Landsat TM by means of leaf area index. Zhang et al. (2002) evaluated the data quality of China - Brazil Earth Resource - 1 satellite through 6 targets of ground resolution, including definition, signal-to-noise ratio, contrast and radiation accuracy. Wang et al. (2007) evaluated the LISS3 image quality of IRS-P6 satellite based on six evaluation indexes, namely radiation accuracy, clarity, information quantity, signal-to-noise ratio, geometric accuracy and ground resolution, and made a comparative analysis based on TM data in the same area. Wei et al . (2012) evaluated the quality of HJ1B-CCD images based on six objective indexes, namely radiation accuracy, information quantity, clarity, signal-to-noise ratio, contrast ratio and ground resolution. Cao (2014) analyzed and evaluated the data quality of Resource no. 1 02C satellite based on the information amount, clarity, gray scale range, noise and other aspects of the data by combining subjective and objective evaluation. Wu et al. (2018) analyzed the hyperspectral data quality of SparK-02 star based on four objective indexes, namely radiation accuracy, signal-to-noise ratio, information entropy and image definition.

In conclusion, there is no systematic study on radiation quality evaluation of OHS data at present. OHS data band with a total of 32 products, if the subjective evaluation method on each assessment will consume a large amount of manpower and material resources and time. Therefore, in this paper, we adopt the method of objective evaluation of the radiation quality evaluation, chose a number of hyperspectral data with a representative feature coverage area respectively, and use the method of objective evaluation: radiation accuracy, resolution, signal-to-noise ratio and the information entropy as the evaluation index, the OHS-2 and OHS-3 to radiation hyperspectral data quality evaluation, and analysis of OHS-2 and OHS-3 different hyperspectral data radiation quality indicators, in hyperspectral data for . This paper provides data quality reference for the application of Zhuhai-1 in geography monitoring, precision agriculture, the state of the wetland resources protection, disaster monitoring and marine environment survey.

2. EVALUATION METHOD OF RADIATION QUALITY

2.1 Image definition

Radiation accuracy is an index reflecting the radiation state of images, including mean value, variance, skewness and steepness. Where, the mean value can reflect the overall radiation condition of the image; The variance reflects the amount of information in the image. The greater the variance, the more abundant the image information will be (Zhang Xia et al., 2002). Skewness and steepness are two indicators reflecting the distribution of image histogram. Skewness reflects the degree to which the distribution shape of image histogram deviates from the symmetric shape around the mean value. Positive and negative values indicate whether the distribution of asymmetric edges tends to be positive or negative. Gradient represents whether the distribution shape of image histogram is concentrated near the mean value or extends to the edge, while concentration near the mean value indicates that the gray scale range of image is narrower. It should be noted that since the gray value of the image is closely related to the type of ground objects, imaging time and weather, the four indexes of radiation accuracy have no absolute significance and can be used for the comparison of the same data without bands. Its calculation formula is shown below:

$$M = \frac{1}{N}\sum_{i=1}^{N} x_i \tag{1}$$

$$d = \frac{1}{N-1}\sum_{i=1}^{N} (x_i - M)^2 \tag{2}$$

$$S = \frac{\sum_{i=1}^{N} \left(\frac{x_i - M}{\sqrt{d}}\right)^3}{N} \tag{3}$$

$$K = \frac{\sum_{i=1}^{N} \left(\frac{x_i - M}{\sqrt{d}}\right)^4}{N} \tag{4}$$

M , d , S , K , x_i , N , represents the the mean value of the image, the variance of the image, Skewness, Kurtosis, the grayscale value of the pixel i and the total number of pixels, respectively.

2.2 Image definition

The image definition is an important index to measure the change of edge of image detail. The higher the sharpness of an image, the more distinguishable the edge details are. In this paper, point sharpening algorithm is used to calculate the clarity (Wang et al., 2004; Wu et al., 2018), the formula is as follows:

$$EVA = \frac{\sum_{i=1}^{N}\sum_{a=1}^{8} \left| df \middle/ dx \right|}{N} \tag{5}$$

EVA , N , df , dx , represents the sharpness of the image, the total number of pixels, the range of gray change of image and the increment of distance between pixels,respectively.

2.3 Signal-to-noise ratio

Signal-to-noise ratio (SNR) reflects the size of useful information and noise information in an image. As one of the important indexes to measure image quality, it is defined as the ratio of the mean value of useful components in an image to the standard deviation of noise components (Gao et al., 2007; Liang et al., 2015; Wu et al., 2018; Zhu et al., 2010). The standard deviation calculation methods of image noise include de-correlation method, local variance method based on Gaussian waveform extraction, local variance method based on edge block elimination, local variance method, etc. (Gao et al., 2007; Zhu et al., 2010). In this paper, the noise is assumed to be gaussian distribution, and the formula for calculating the image SNR of gaussian distribution is:

$$SNR = \frac{m}{\delta} \tag{6}$$

SNR , m , δ , represents the signal-to-noise ratio of the image, the mean value of pixels, and the standard deviation,respectively.

2.4 Information entropy

Information entropy is an important index to reflect the amount of information contained in an image, which can reflect the level of detail of the information contained in the image. Generally speaking, the higher the information entropy is, the more information the image contains and the more detailed the feature information is. Common entropy includes Shannon entropy, conditional entropy, square entropy and cubic entropy, etc. In this paper, Shannon entropy is used to represent the amount of information in OHS hyperspectrum. Shannon entropy is calculated as follows:

$$H = -\sum_{i=\min}^{\max} p_i \log_2 p_i \tag{7}$$

H ,min, max, p_i , represents Information entropy of image, Image gray minimum, Image gray maximum and the probability of the pixel of grayscale value i ,respectively.

3. STUDY AREA

In this study, The L1 hyperspectral image data were selected from two different satellites, OHS-2A and OHS-3D, with a spatial resolution of 10m and 2.5nm. In order to avoid the influence of land cover types, three regions with different land cover types and complexity were selected for quality evaluation with data size of 2000×2000 pixels. The experimental area of OHS-2A was marked as A, and three areas were selected near Erhai Lake, Dali, Yunnan, Renqiu City, Hebei and Xiuwen County, Guizhou. The main surface types were water bodies, farmland and forest land, as shown in Fig.1A. The false color was synthesized as R (880nm), G (670nm) and B (566nm). The OHS-3D experiment area is marked as B, and the three areas are: near Zhongshan city, Guangdong Province, Yulin City, Shaanxi Province and Dongting Lake, Hunan Province. The main surface cover types are towns, forest land, water body and farmland, as shown in FIG. 1b. The false color synthesis is R

(880nm), G (670nm) and B (560nm).

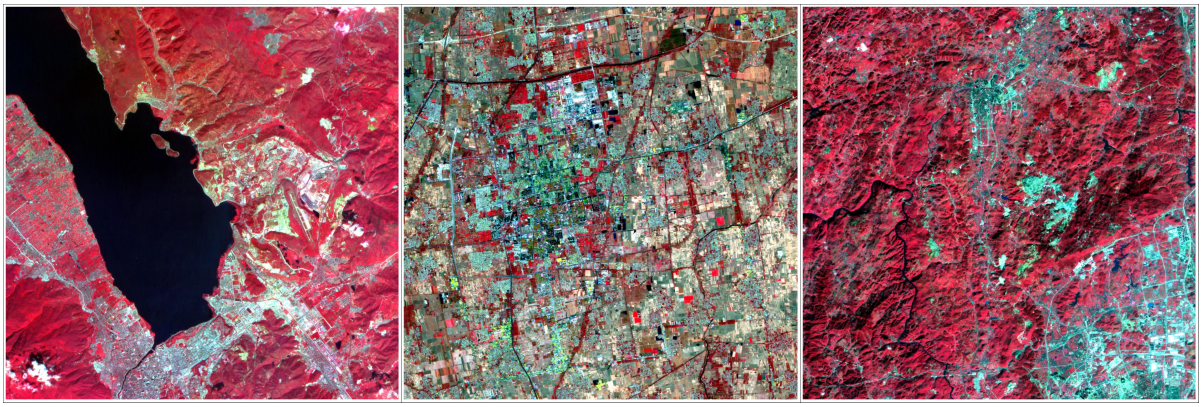

A (1) Dali, Yunnan (2) Renqiu, Hebei (3) Xiuwen, Guizhou

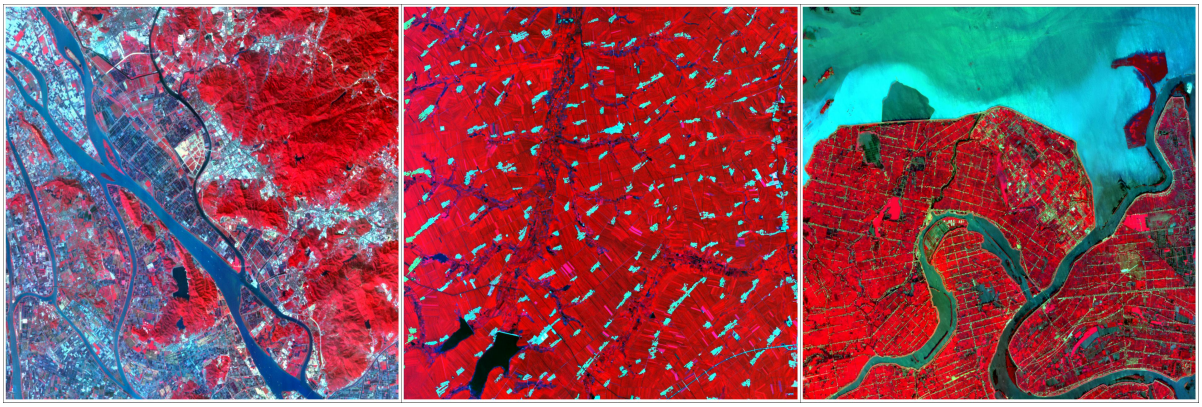

B (1) Zhongshan, Guangdong (2) Yulin, Shanxi(3) Dongting Lake, Hunan

Fig.1 False-color display of Zhuhai Hyperspectral data in different area

4. RESULTS

4.1 Evaluation results of OHS-2A

The precision of OHS-2A satellite radiation is shown in Fig.2. In OHS-2A, the mean curve of different land cover types keeps the same trend, showing a decreasing trend at 466-656nm, and basically maintaining a stable trend at 820-866nm. However, in the variance index, Dali is much higher than the variance of other regions and is not on the same order of magnitude, resulting in the variance of other regions showing approximate horizontal lines. For Dali region, there were two different trends at 466-716nm and 730-946nm. In the 466-716nm spectrum segment, the variance remained stable, while in the 730-946nm spectrum segment, the variance showed a complex trend. After magnifying the variance results of the other two regions, it was found that the variance showed a decreasing trend in the 730-946nm spectrum segment. In terms of skewness and steepness index, different land cover types show similar trends. In the 466-730nm spectrum segment, skewness and steepness showed a decreasing trend, while in the 730-946nm spectrum segment, skewness and steepness showed a stable trend, indicating that the distribution of OHS-2A histogram was basically consistent in different land cover types. For the edge radiation distortion and gain adjustment distortion, the OHS-2A shows a consistent trend. As Dali's edge radiation distortion and gain adjustment distortion range from 0-1, which is quite different from other land cover types, it presents an approximate horizontal line, while other areas are reduced first and then remain stable at 746nm-866nm. In conclusion, the radiation accuracy of OHS-2A shows a consistent trend in the

red-green-blue spectrum, and remains consistent in the near-infrared spectrum.

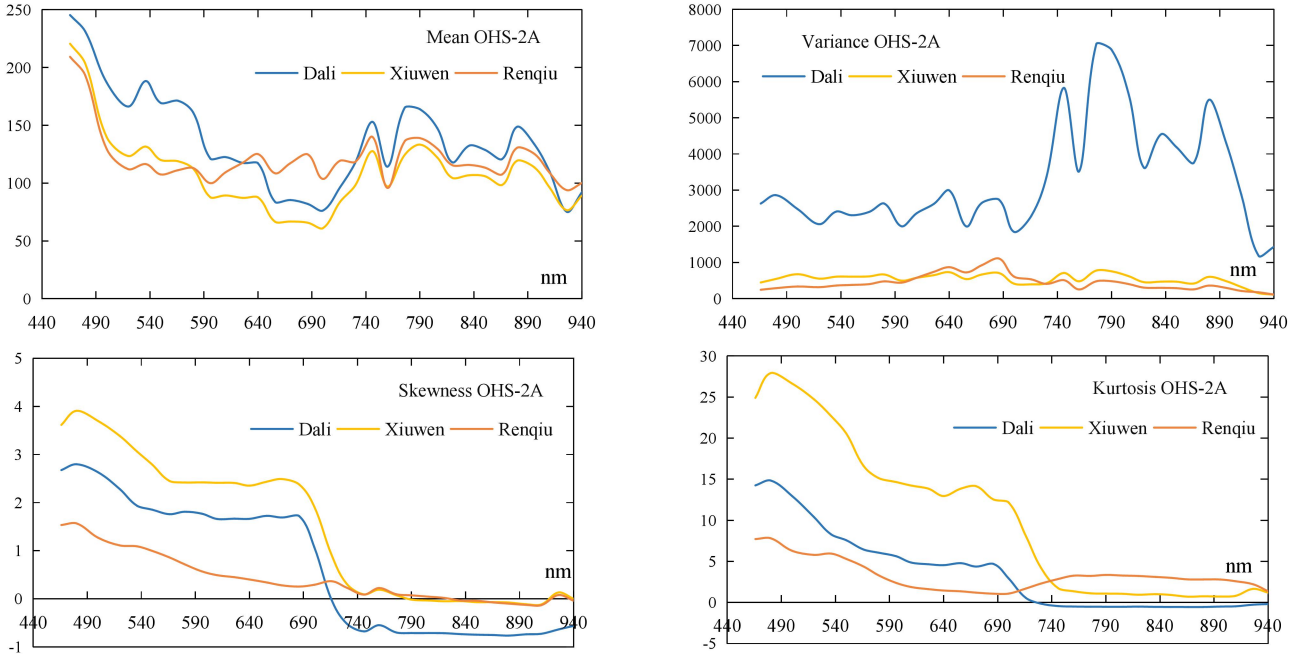

Fig.2 Radiation accuracy of OHS-2A

The computed results of the satellite definition of OHS-2A are shown in Figure 3. The trend of the definition curves of different surface cover types is consistent, and the overall definition is above 24. A total of three peaks appear, namely 686nm, 776nm and 880nm. In the infrared band, 880-940nm shows an obvious trend of decrease. Therefore, the spectral data of 880-940nm can be removed in the application.

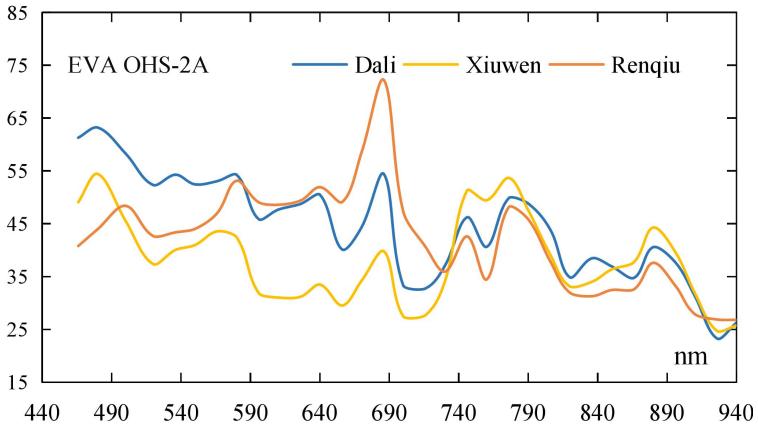

Fig.3 Image definition of OHS-2A

The results of SNR calculation are shown in Fig. 4. For OHS-2A satellite data, the SNR curve of different surface cover types keeps the same trend. In the spectral segment of 440nm-686nm, the SNR of surface features of different surface types presents a decreasing trend; in the spectral segment of 686nm-746nm, the SNR presents an increasing trend; in the spectral segment of 746nm-896nm, the SNR of surface features basically remains unchanged. It should be noted that in the OHS-2A star hyperspectral data, the SNR of water image is distributed between 1-5, and that of towns, woodlands and farmland is distributed between 2-14. At the same time, at the same SNR calculation method, based on the EO-1 Hyperion hyperspectral data signal-to-noise ratio in the range of 0 to 4 (2008) Zhou Yu ji and qing-jiu tian, HJ1B data signal-to-noise ratio in the range of 2-5 (hong-wei wei and qing-jiu tian 2012), the IRS - P6 P6 (India) satellite signal to noise ratio of 1 to 7 (qin-jun wang and qing-jiu tian 2007, while the signal-to-noise ratio of the high score - 1/2 1-8

cai-yun zeng (2017), by contrast, OHS-2A satellite with the same level of SNR.

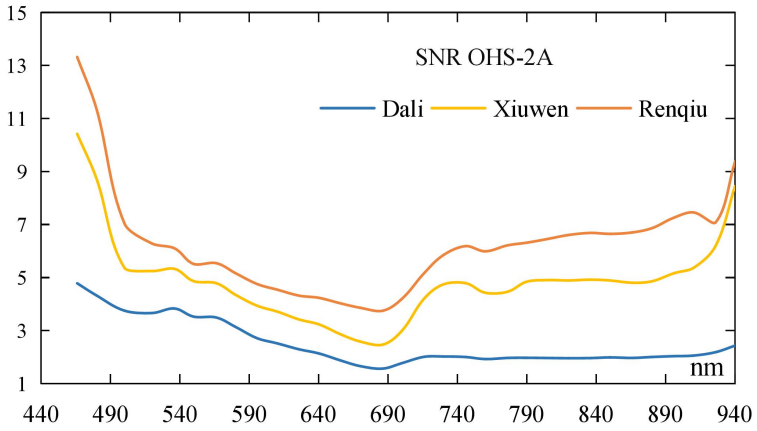

Fig.4 Signal to Noise Ratio of OHS-2A

Fig. 5 shows the calculation of information entropy. In OHS-2A, the information entropy of all spectral segments is above 5.4 and basically remains stable, that is, the information of all spectral segments is basically consistent. Since the gray value variance of all bands in the Dali area is greater than that of the other two regions, the images in this area contain a large amount of information, so the information entropy is greater than that of other land cover types, that is, the OHS-2A satellite data can express rich water information. In the spectrum segment of 890nm-940nm, the information entropy presented a decreasing trend, but the Dali region presented a trough at 910nm. Meanwhile, the Shannon information entropy of EO-1 Hyperion data (Zhou Yuji and Tian Qingjiu 2008) is between 5-12, HJ1B data Shannon information entropy is between 1-2 (Wei Hongwei and Tian Qingjiu 2012), and SPARK hyperspectral data Shannon information entropy is between 3-7 (Wu Xing et al., 2018). It can be seen that Zhuhai OHS-2A data has a high information entropy.

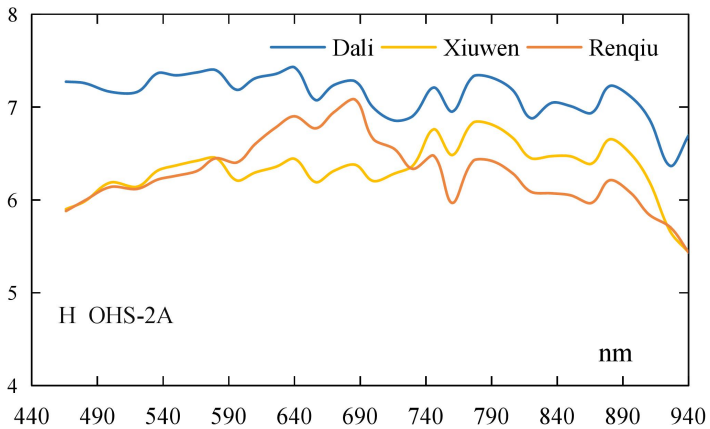

Fig.5 Shannon Entropy of OHS-2A

4.2 Evaluation results of OHS-3D

The precision of OHS-3D satellite radiation is shown in Figure 6. In the OHS-3D, in the mean index, the cut-off point is 730nm. In the blue, green and red spectrum segments, the mean values of different land cover types all show a trend of decrease, while in the 746-880nm range, the mean values basically remain stable, and in the 896-940nm range, the mean values show a trend of decrease. For the variance index, in 443-730nm, show the increasing trend of Dongting lake, Zhongshan showed increased after decreased trend, then the Yulin showed the trend of relatively stable (in addition to 670nm, showed the maximum value), in 740-940nm, Yulin and Zhongshan

area show the variance trend of stability, and shows the trend to increase after the first reduce of Dongting lake area. Especially at 940nm (32 band), images of different types of land cover all show the minimum variance, indicating that the gray scale range of the last band is relatively narrow. Zhongshan and dongting lake and show a consistent trend and gradient of skewness, in 443-73nm, showed a higher degree of partial, in 746-940nm showed lower partial degrees, Yulin area in 746-880nm showed high skewness and steepness, tend to be more negative, the edge of asymmetric distribution and the dynamic range of gray level and more narrow, other surface coverage types of gray dynamic range is wide; Distortion and gain adjustment for edge radiation to all areas on the final band which is 940nm showed a high degree of heterogeneity, indicating a large noise, for the Dongting lake area and Zhongshan, in the other spectrum shows the degree of heterogeneity, low for Yulin area, in 746-940nm, showed a larger value. In conclusion, the radiation accuracy of OHS-3D shows a consistent trend in the red-green-blue spectrum, and the 896-940nm spectrum has a high noise, especially for farmland surface cover types.

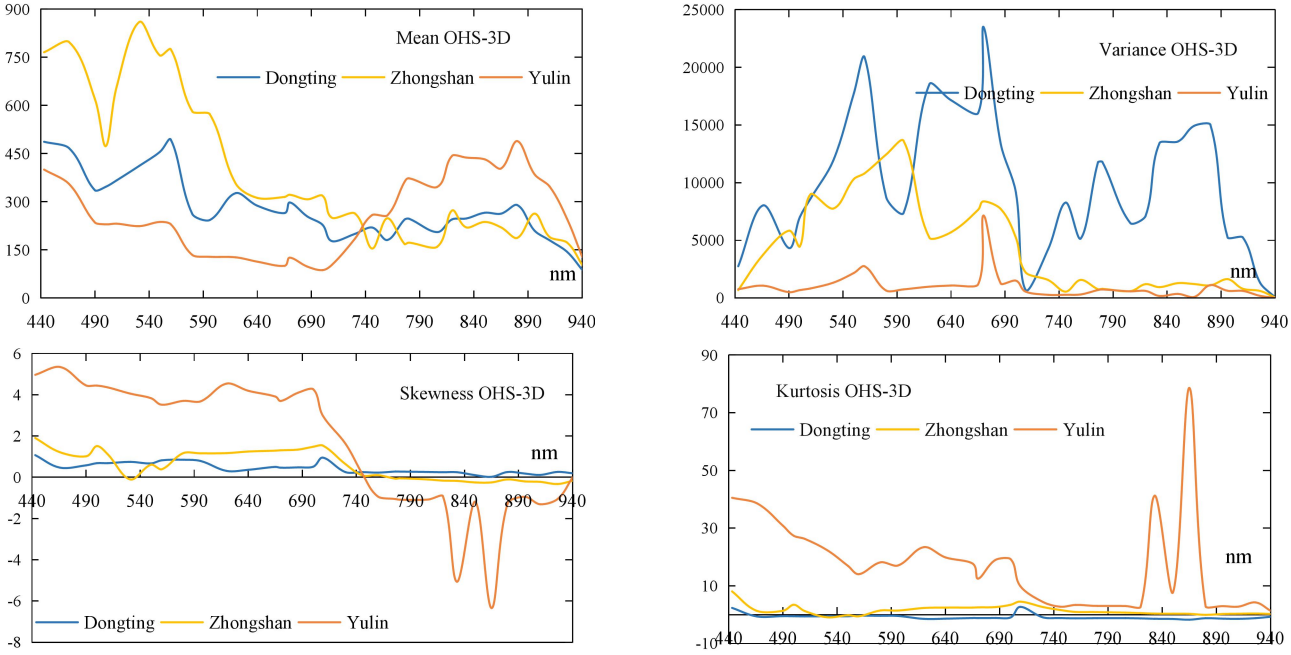

Fig.6 Radiation accuracy of OHS-3D

The computed results of OHS-3D definition are shown in Fig.7. The spectral range of 443-709 shows a higher definition, the spectral range of 730-940nm shows a lower definition, but it is basically above 16. The spectral range of 896-940nm (29-32 band) shows a significant reduction trend, and the last band shows a minimum value. At the same time, the definition curve of different land cover types is basically consistent, indicating that THE definition of OHS-3D is basically consistent in different land cover types. At the same time, two peaks appeared in areas of different land cover types. The first one of the three regions all appeared at 550nm, with the definition of 122.9, 135.2 and 55.5, respectively. The second crest, however, showed a backward shift, but it was all distributed in the red wave band, of which yulin region appeared at 670nm (band 14) with a value of 68.2, Zhongshan region appeared at 686nm (band 15) with a value of 98.0, and Dongting Lake region appeared at 700nm (band 16) with a value of 118.2.

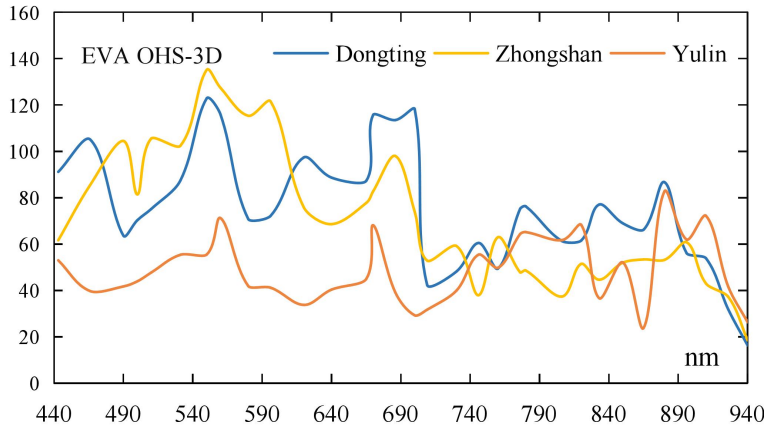

Fig.7 Image definition of OHS-3D

The results of the OHS-3D star SNR calculation are shown in Fig. 8. The SNR curves of different land cover types keep the same trend in the 443-833nm spectrum segment, and show a decreasing trend in the 443-700nm spectrum segment. In the stable region of Zhongshan and Dongting Lake at 850-940nm, Yulin shows a high SNR at 833-865nm, indicating that the spectrum at 833-856nm has a high farmland information content, which can be used for crop information estimation, etc. Meanwhile, in comparison with EO-1 Hyperion data, HJ1B data, IRS-P6 (India P6) satellite data and high-resolution 1/2 data based on the same SNR calculation method (Wang et al.2007; Wei et al. 2012; Zhou et al. 2008), OHS-3D stars have the same level of SNR.

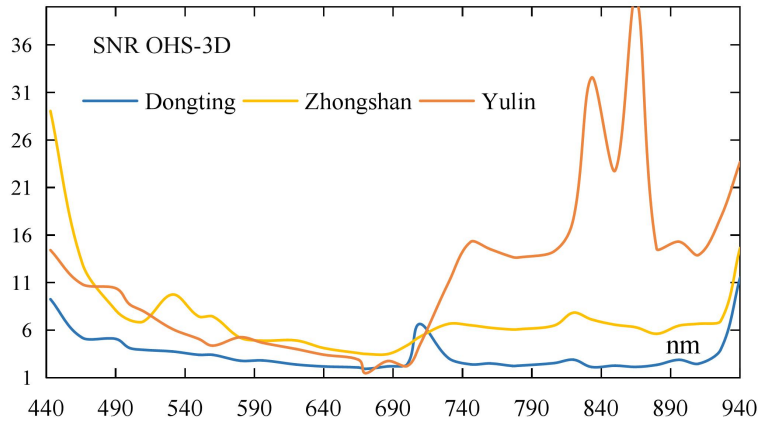

Fig.8 Signal to Noise Ratio of OHS-3D

OHS-3D star information entropy calculation is shown in figure 9, all of the information entropy spectrum in 4.5 above, in the 896-940nm (29-32) band spectrum, information entropy presents a decreasing trend, and in the last period of 940nm show a spectrum minimum information entropy, indicates that the final spectrum contains the amount of information is less than the previous spectrum, spectrum and noise contained the earlier period of higher, at the same time and the EO 1 Hyperion data, HJ1B data and SPARK hyperspectral data of Shannon information entropy was basically the same level, However, OHS-3D data has a high Shannon information entropy (Wang et al.2007; Wei et al. 2012; Zhou et al. 2008).

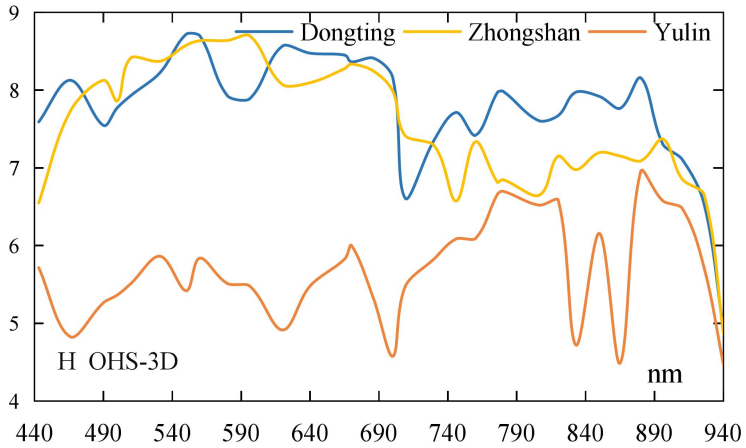

Fig.9 Shannon Entropy of OHS-3D

4.3 Comparative analysis of OHS-2A and OHS-3D

In order to comprehensively reflect the overall trend of radiation quality of different OHS satellite data, this paper calculated the average values of each evaluation index in three different types of land cover data, and then divided them into blue, green, red and near-infrared groups according to the spectrum segment. The maximum, average and minimum values of each index group were calculated respectively.

The comparison of sharpness are shown in Fig.10. The EVA value is maintained above 20. The EVA of OHS-2A in the blue and green bands is basically stable, while the EVA of OHS-3D in different bands varies greatly, and the EVA of OHS-3D in the green band is the largest, while the EVA of OHS-3D in the near infrared band is poor. In the blue, green and red spectra, the maximum, average and minimum values of the definition of OHS-3D are all greater than that of OHS-2A . However, in the near infrared spectrum segment, the minimum definition of OHS-2A is greater than that of OHS-3D, while the maximum and average value are that of OHS-3D is greater than that of OHS-2A. This indicates that although OHS-3D is affected by the noise in the last four bands, the overall definition of OHS-3D is higher than that of OHS-2A.

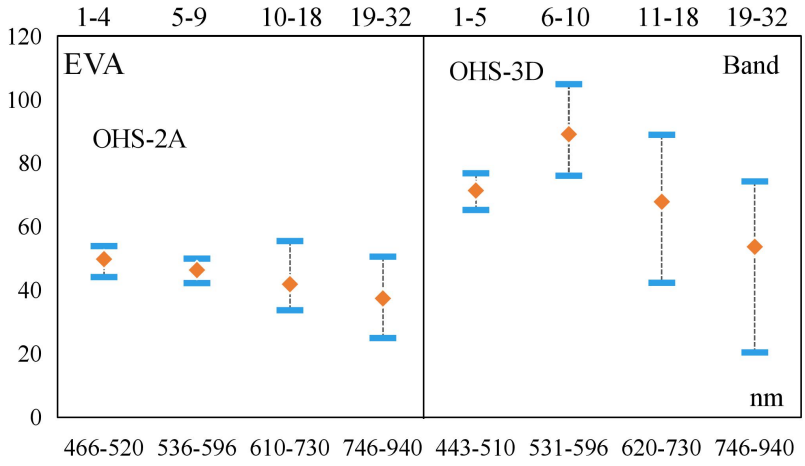

Fig.10 Comparison of Image definition between OHS-2A and OHS-3D

As shown in FIG. 11, OHS-2A has the minimum SNR in the red band, while OHS-3D star has the same phenomenon. In the blue, green, red and near-infrared spectra, the maximum and average SNR of OHS-3D were all greater than that of OHS-2A, indicating that the information content of OHS-3D was higher than that of OHS-2A .

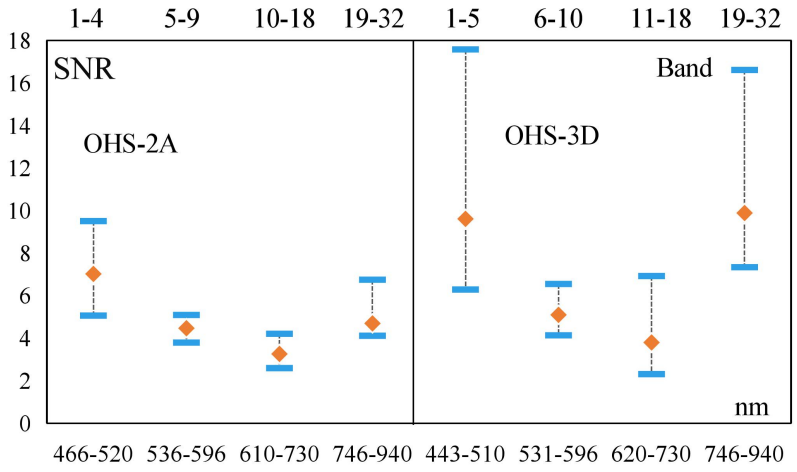

Fig.11 Comparison of Signal to Noise Ratio between OHS-2A and OHS-3D

The comprehensive evaluation and comparison of information entropy are shown in FIG. 12.

The information entropy of OHS-2A is above 5.5, while that of OHS-3D is above 4.5. Consistent with the definition, in the blue, green and red spectral segments, the maximum and average information entropy of OHS-3D is greater than that of OHS-2A star. In the near infrared spectrum segment, the minimum value of OHS-2A information entropy is greater than that of OHS-3D, while the maximum and average value are that of OHS-3D is greater than that of OHS-2A. This indicates that although the noise of the last four bands of OHS-3D is relatively large, the overall information entropy of OHS-3D is higher than that of OHS-2A.

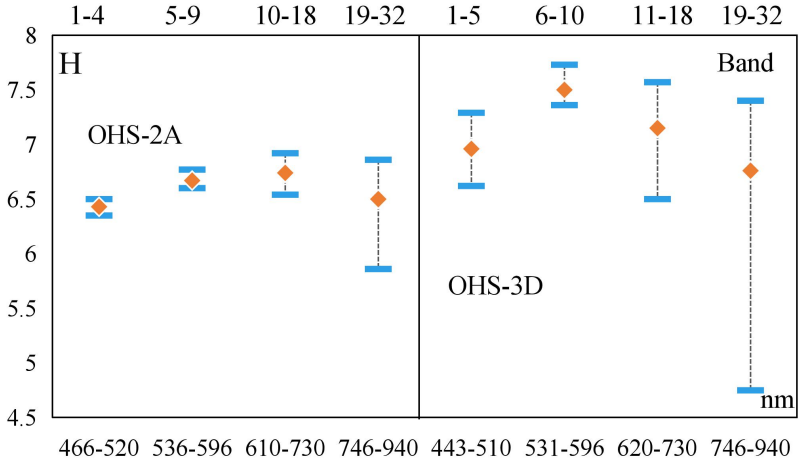

Fig.12 Comparison of Shannon Entropy between OHS-2A and OHS-3D

The above analysis shows that in blue, green and red spectrum, OHS - 3D's radiation, accuracy, resolution, signal-to-noise ratio and information entropy are higher than that of OHS-2A, but in the near infrared spectrum, due to the OHS-3D in the 896-940nm spectrum of noise influence, causes of OHS-2A clarity and information entropy minimum value is higher than the OHS-3D, but for the average and maximum, OHS-3D is still higher than that of OH-2A. In summary, the radiation quality of OHS-3D is better than that of OHS-2A .

5. CONCLUSION

In this paper, the radiation quality of OHS image data is evaluated by four evaluation indexes, including radiation accuracy, clarity, signal-to-noise ratio and information entropy, and the data quality of OHS-2A and OHS-3D is compared and analyzed. The result shows that OHS data has a good quality of radiation in the red, green and blue spectral section, and OHS-3D radiation quality is better than OHS-2A. Due to the signal-to-noise ratio and information entropy of the OHS data are at the same level as EO-1 and HJ1B datal, and the revisit cycle of OHS data is higher, the complementarity of OHS data and other data can be considered in application.

The OHS data has abundant information in the feature bands of vegetation, it can reflect the key phenological information of vegetation and crops due to its high temporal resolution. Therefore, the OHS data has immeasurable application potential in agricultural remote

sensing. Because our country inland/near-shore waters have considerable degree of spatial variability and time variability, such as WFI in GF - 1 16 m spatial resolution based on the data, there are about 15% - 20% of the small space scale change information (Li 2015). Therefore, high spatial resolution (10 m) and high revisit cycle (2 days) of the OHS data will have an irreplaceable role in our country inland/offshore water quality monitoring. In the future, the radiation sensitivity of OHS data for quantitative monitoring of water environmental parameters will be studied aiming at quantitative application of inland water bodies.

Reference:

Forster B C, Best P. 1994. Estimation of SPOT P-mode point spread function and derivation of a deconvolution filter. ISPRS Journal of Photogrammetry and Remote Sensing, 49(6):32-42. [DOI: 10.1016/0924-2716(94)90013-2]

Kamal M, Phinn S, Johansen K. 2016 Assessment of multi- resolution image data for mangrove leaf area index mapping. Remote Sensing of Environment, 176: 252-254. [DOI: 10.1016/j.rse.2016.02.013].

Cao C X. 2014. Date Quality Evaluation of ZY-I-02C Satellite. Beijing: China University of Geosciences

Zeng C Y. 2017. The Quality Assessment and Feature Analysis of Domestic High Resolution Satellite Images. Chengdu: Chengdu University of Technology.

Gao L R, Zhang B, Zhang X, Shen Q. 2007. Study on the Method for Estimating the Noise in Remote Sensing Images Based on Local Standard Deviations. Journal of Remote Sensing, 11(2) :201-208.

He N N, Xie K, Li T, Ye Y S. 2017. Overview of Image Quality Assessment. Journal of Beijing Institute of Graphic Communication, 25(2):47-50.

Hong Tao. 2019. Research on the Inland lake monitoring based on OHS. Satellite Application, (8):19-22.

Li J. 2015. Research on spatial-temporal-radiometric requirements for quantitative remote sensing of highly dynamic coastal/inland waters. Wuhan: Wuhan University.

Li X Y, Fan H S, Pan S L, Jiang X H, Wu J Q. 2019. Application of Zhuhai No. 1 hyperspectral satellite data. Satellite Application, (8):12-18.

Liang W X, Li J S, Zhou D M, Shen Q, Zhang F. F. 2015. Evaluation of GF-1 WFV Characteristics in Monitoring Inland Water Environment. Remote Sensing Technology and Application, 30(4): 810-818.

Ren X. 2008. Research and Implement of Objective Image Quality Evaluation Model. Nanjing: Nanjing University of Aeronautics and Astronautics.

Sun H R, Zhao Z G, Zhao J X, Chen W W. 2020. Inversion of Topsoil Organic Matter Content by Hyperspectral Remote Sensing of Zhuhai-1. Remote Sensing Information, 35(4):40-46.

Wang H N, Zhong W, Wang J, Xia D S. 2004. Research of Measurement for Digital Image Definition. Journal of Image and Graphics, 9(7): 828-831.
Wang Q J, Tian Q J. 2007. Quality Evaluation of LISS3 Image from IRS-P6 Satellite. Geography and Geo-Information Science, 23(3):11-14.
Wang X P, Zhang J, Ma Y, Ren G B. 2016. Image Quality Evaluation for ZY-1 02C Satellite in Coastal Zone Area. Advances in Marine Science, 34(1): 129-137.
Wei H W, Tian Q J. 2012. Quality Evaluation and Analysis of HJ1B-CCD images. Remote sensing information, 27(5): 31-36.
Wu X, Zhang X, Sun X J, Zhang L F, Qi W C. 2018. Radiation Quality Evaluation of Spark Hyperspectral Satellite Image. Remote Sensing Technology and Application, 33(2): 233-240.
Yin H X, Fan Y G. 2020. Research on the Extraction Method of Water in Erhai Lake based on OHS-2A. Spacecraft Recovery & Remote Sensing, 41(4):118-127.
Yin L Z, Zhu J, Cai G L, Wang J H. 2014. Review on Quality Evaluation Methods of Remote Sensing Image. Geomatics & Spatial Information Technology, 37(12):32-35.
Zhang X, Zhang B, Zhao Y C, Tong Q X, Zheng L F. 2002. Image Quality Assessment for the Infrared Multi-Spectral Scanner of the Chinese-Brazil Earth Resources Satellite. Journal of Image and Graphics, 7(6): 581-586.
Zhang X Y, Li J X. 2019. Research on the Crops elaborate classification of Gaomi based on OHS. Satellite Application, (8):29-33.
Zhou J C, Dai R W, Xiao B H. 2008. Overview of Image Quality Assessment Research. Computer Science, 35(7):1-4.
Zhou Y J, Tian Q J. 2008. Image Quality Evaluation of EO-1 Hyperion Sensor, 10(5):678-683.
Zhu B, Wang X H, Tang L L, Li C R. 2010. Review on Methods for SNR Estimation of Optical Remote Sensing Imagery. Remote Sensing Technology and Application, 25(2):303-309.